Katherine Klein[1] *and J. Carlos Santamarina*[1]

Methods for Broad-Band Dielectric Permittivity Measurements (Soil-Water Mixtures, 5 Hz to 1.3 GHz)

REFERENCE: Klein, K. and Santamarina, J. C., **"Methods for Broad-Band Dielectric Permittivity Measurements (Soil-Water Mixtures, 5 Hz to 1.3 GHz),"** *Geotechnical Testing Journal*, GTJODJ, Vol. 20, No. 2, June 1997, pp. 168–178.

ABSTRACT: Broad-band permittivity data enable the determination of micro- and macro-scale material characteristics and the monitoring of geo-processes. While high-frequency (>≈100 MHz) permittivity measurements can be performed readily in the laboratory, low-frequency (<≈10 MHz) measurements are more difficult to conduct. This paper describes two low-frequency techniques and presents broad-band permittivity data for various soil-water mixtures.

Low-frequency data were gathered with an impedance analyzer in conjunction with two-terminal and four-terminal measurement systems. The two-terminal cell consisted of two copper electrodes; its range was restricted at low frequencies due to electrode polarization. The four-terminal system used separate current and voltage electrodes; its accuracy at low frequencies was limited by the ability of the equipment to resolve small phase angles.

High-frequency data obtained with a coaxial termination probe and low-frequency data obtained with these two cells are presented. Soils of very different specific surface were tested at water contents ranging from air-dry to saturated. It is shown that the conductivity of the specimen controls not only the low-frequency measurement limit (i.e., electrode polarization and phase resolution), but also the high-frequency limit due to stray inductances.

KEYWORDS: dielectric, permittivity, conductivity, resistivity, soils, colloids, electrolytes

Notation

α	Polarizability
β	Fitting parameter for constant phase element
δ	Loss angle
ϵ^*	Complex dielectric permittivity ($C^2/J \cdot m$)
ϵ', ϵ''	Real and imaginary dielectric permittivity ($C^2/J \cdot m$)
ϵ_o	Dielectric permittivity of free space ($8.8541878 \cdot 10^{-12}$ $C^2/J \cdot m$)
κ^*	Complex relative dielectric permittivity ($\kappa^* = \epsilon^*/\epsilon_o$)
κ', κ''	Real and imaginary relative dielectric permittivity
κ'_{inf}	Real dielectric permittivity at frequencies much greater than relaxation frequency
κ'_{st}	Real dielectric permittivity at frequencies much less than relaxation frequency
$\kappa'' + \sigma/\omega\epsilon_o$	Losses
$\kappa''\omega\epsilon_o + \sigma$	"Effective conductivity"
σ	Conductivity, S/m
τ	Relaxation time, s
θ	Phase angle
ω	Angular frequency, rad/s
A	Area, m^2
C	Capacitance, F
c	Concentration, mol/m^3
d_1, d_2	Normalized thickness ($d_1 + d_2 = 1$)
E	Electric field intensity, V/m
e	Electrode
F	Faraday's constant (96484.6 C/mol)
f	Frequency, Hz
H_c	High current terminal
H_p	High potential terminal
I	Current, A
J	Current density, A/m^2
j	Represents imaginary component ($j = \sqrt{-1}$)
L	Length, m
L_c	Low current terminal
L_{cable}	Cable inductance
L_p	Low potential terminal
M	Fitting parameter for constant phase element
m, meas	Measured value
mix	Mixture
model	Modeled value
N	Fitting parameter for constant phase element
n	Number of measurements
N_{AV}	Avogadro's number ($6.02 \cdot 10^{23}$ mol^{-1})
Q	Constant phase element
R	Resistance, Ω
s	Specimen
S_s	Specific surface of particles, m^2/g
u	Ionic mobility, $m^2/V \cdot s$
wc	Water content, %
Y	Admittance, S
Z	Impedance, Ω

Introduction

Non-destructive, electromagnetic wave-based technologies can be used to obtain micro-level information about soils, including

[1]Graduate student and associate professor, Georgia Institute of Technology, Atlanta, formerly University of Waterloo, Ontario.

moisture content, soil composition, and electrolyte composition, as well as to monitor geo-processes such as diffusion of concentration fronts, consolidation, and cementation. Electromagnetic waves can also provide information about the spatial distribution of materials and interactions between phases in multi-phase mixtures.

The permittivities of geomaterials have been studied in various fields including agriculture, space programs (for the remote evaluation of the Earth and other planets), geophysics, and geotechnical engineering. Current needs for near-surface assessment, concerns about geoenvironmental issues, and the availability of versatile measurement devices [e.g., ground-penetrating radar (GPR) and time domain reflectometry (TDR)] have revived the interest in measuring and understanding the permittivity of geomaterials.

Laboratory permittivity measurements at high frequencies ($f > \approx 100$ MHz) can be performed very efficiently with commercially sold impedance analyzers and probes (Fam and Santamarina 1995). However, low-frequency permittivity measurements ($f < \approx 10$ MHz) of moist soils remain challenging. This paper provides details about two low-frequency measurement techniques. It also presents broad-band frequency data for various soil-water mixtures that were obtained using these two systems and a high-frequency measurement device.

Review of Polarization and Permittivity

Dielectric permittivity is a measure of the polarizability of a material. Polarization is the spatial separation of charges due to an applied electric field. The mechanisms that cause polarization depend on the frequency of the applied electric field and the composition of the material. Single-phase, homogeneous materials experience only high-frequency polarization mechanisms: electronic, ionic, and molecular (von Hippel 1954). Multi-phase, heterogeneous materials experience these polarization mechanisms, as well as low-frequency polarizations: interfacial-spatial, bound water, and double layer (Sumner 1976; Parkhomenko 1967). Bound-water and double-layer polarizations reflect interactions between phases (de Loor 1983; Santamarina and Fam 1997).

If the polarization of a two-phase material is due to the movement of ions, the permittivity is a function of the conductivity of the phases. The simplest relationship between permittivity, κ^*, and conductivity, σ, is captured in Maxwell's interfacial polarization model for a two-phase, layered medium (von Hippel 1954):

$$\kappa'_{mix} = \kappa'_{inf} + \frac{\kappa'_{st} - \kappa'_{inf}}{1 + \omega^2\tau^2} \tag{1}$$

$$\kappa''_{mix} = \frac{(\kappa'_{inf} - \kappa'_{st})\omega\tau}{1 + \omega^2\tau^2} - \frac{\sigma_{mix}}{\omega\epsilon_o} \tag{2}$$

where the single quote indicates real permittivity and the double quote indicates imaginary permittivity. τ is the relaxation time and ϵ_o is the permittivity of free space ($8.85 \cdot 10^{-12}$ C^2/J·m). The subindices imply: "mix" for mixture, "inf" for frequencies much greater than the relaxation frequency, and "st" for frequencies much lower than the relaxation frequency. These parameters are defined in terms of the real permittivity of the phases (κ'_1 and κ'_2), their conductivities (σ_1 and σ_2), and normalized thicknesses (d_1 and d_2, such that $d_1 + d_2 = 1$):

$$\kappa'_{inf} = \left(\frac{d_1}{\kappa'_1} + \frac{d_2}{\kappa'_2}\right)^{-1} \tag{3}$$

$$\kappa'_{st} = \frac{\kappa'_1 d_1 \sigma_2^2 + \kappa'_2 d_2 \sigma_1^2}{(\sigma_1 d_2 + \sigma_2 d_1)^2} \tag{4}$$

$$\tau = \frac{\kappa'_1 d_2 + \kappa'_2 d_1}{\sigma_1 d_2 + \sigma_2 d_1} \tag{5}$$

$$\sigma_{mix} = \left(\frac{d_1}{\sigma_1} + \frac{d_2}{\sigma_2}\right)^{-1} \tag{6}$$

From a microscopic viewpoint, the conductivity of a single-phase material σ (S/m) is directly related to the ionic mobility u (m^2/V·s):

$$u = \frac{\sigma}{c|z|F} \tag{7}$$

where c is ionic concentration (mol/L), z is ionic valence ( ), and F is Faraday's constant (9648.6 C/mol). Similarly, the real permittivity κ' is a function of the polarizability of elemental charges α. The Clausius-Massoti equation predicts (von Hippel 1954):

$$\kappa'_1 = \frac{1 + \frac{2}{3\epsilon_o} N_{AV}\alpha}{1 - \frac{N_{AV}\alpha}{3\epsilon_o}} \tag{8}$$

where N_{AV} is Avogadro's number and α is the average dipole moment per unit field strength. Therefore, macroscopic permittivity measurements reflect microscopic material properties such as ionic mobility and polarizability.

Two-Terminal Electrode Systems (Hz-MHz)

The two-terminal system consists of two parallel disk electrodes. Each electrode is both a current and a potential terminal (Fig. 1). The electrical properties of the specimens are determined by measuring the electric field E between the high potential, H_p, and low-potential, L_p, electrodes, and the applied current I across the high-current, H_c, and low-current, L_c, electrodes, and computing the resultant transfer function.

The most significant error at low frequencies associated with the two-terminal measurement system is electrode polarization. This is an interfacial impedance in series with the specimen impedance, which is the result of charge accumulation at the electrode-

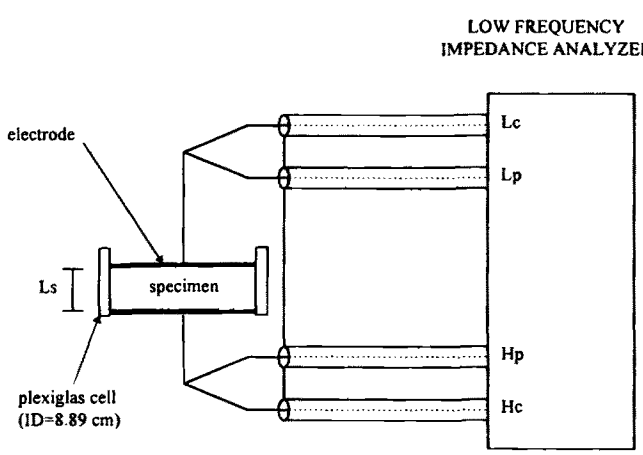

FIG. 1—*Two-terminal system: The sample holder includes two disk-shaped copper electrodes and an external plexiglas cylinder.*

specimen interface: ionic conduction within the material is incompatible with electron conduction in the peripheral electronic circuitry (electrodes, cables, and measurement system), causing an ionic diffuse layer to build at the electrode. Oxidation-reduction reactions at the electrode-material interface and ionic diffusion within the diffuse layer reduce this interfacial accumulation of charges. If redox reactions and ionic diffusion do not occur, the capacitive impedance at the soil-electrode interface decreases with increasing frequency, $Z \propto f^{-1}$. Redox impedance may be represented by the reaction resistance, $Z \propto f^{0}$. Ionic diffusion impedance decreases with the square root of frequency, $Z \propto f^{1/2}$ (Ward 1992).

Materials used for electrodes include: rigid metals (e.g., copper), metal foil, conducting paints, fired-on silver, sprayed metal, evaporated metal and plasmas, sputtered electrodes, liquid metal, water, and reversible electrode systems (ASTM 1987; Scott et al. 1967). The preferred electrode materials are stable metals (e.g., gold and platinum) because they eliminate electrochemical redox effects; yet the use of non-reactive or "blocking" electrodes magnifies other electrode polarization effects. Electrode polarization (i.e., ion blocking, redox reactions, and ionic diffusion) affect the computed values of complex permittivity and conductivity.

Different methods have been suggested to eliminate or minimize electrode polarization effects: reversible electrodes (Scott et al. 1967), measurements at two different sample lengths (Schwan 1962; Hill et al. 1969), insulating layer (Gross and McGehee 1988), and substitution techniques (Schwan 1962; Hill et al. 1969). The analysis of electrode polarization with models similar to those used in this paper readily show that these alternatives are ineffective and unreliable.

Other errors in the two-terminal system are: fringe/edge capacitance, which is due to the non-uniform electric field near the edge of the capacitor and around the specimen, and surface conduction effects. Both errors increase as the ratio of specimen thickness to diameter increases and can be controlled through the use of a guard electrode (ASTM 1987).

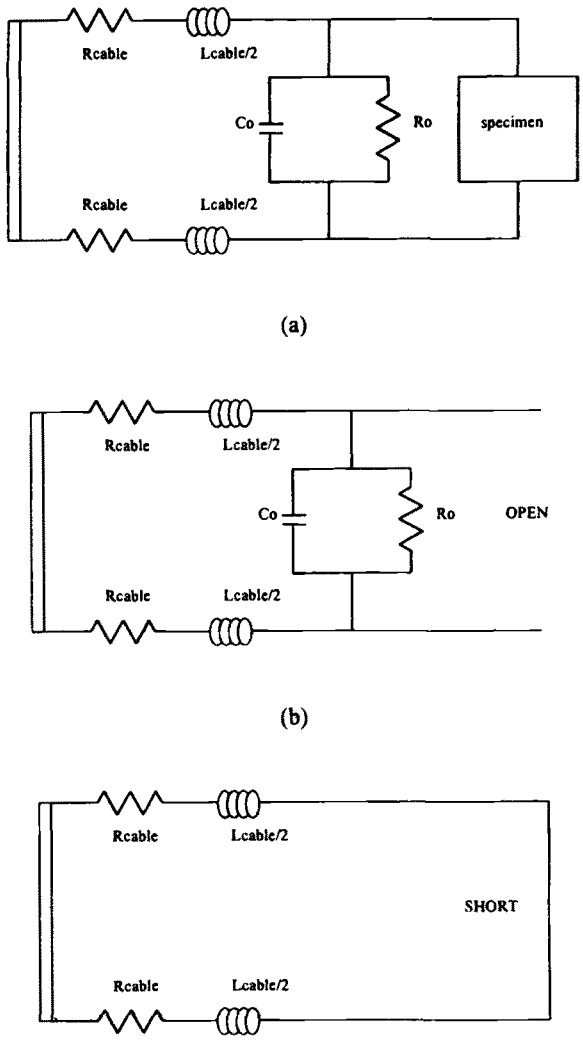

FIG. 2—*Calibration of the two-terminal system:* (a) *residual and stray parameters:* (b) *open circuit;* (c) *short circuit.*

Experimental Setup

The two-terminal specimen holder used in this study consisted of two circular copper electrodes (diameter = 8.89 cm), a plexiglas cylinder (same diameter as the electrodes) that fit over the electrodes, and o-rings to hold soil-and-fluid specimens in place. The specimen was placed between the two electrodes, and the specimen holder was connected to an HP-4192A impedance analyzer through four terminals: high-current, H_c, high-potential, H_p, low-current, L_c, and low-potential, L_p, connectors. The configuration of the leads and the connection of the shields are shown in Fig. 1. The HP-4192A measures two independent impedance parameters, but can display the results in several formats. It is recommended that impedance Z or admittance Y and phase angle θ be measured to avoid problems with measurement ranges. Other parameters can be calculated from these values.

Calibration

Figure 2*a* shows the residual parameters associated with the test fixture. These parameters must be removed from the measured impedances to obtain the true impedance of the specimen. Calibration measurements were performed in open-circuit (i.e., air as the dielectric) and short-circuit (i.e., electrode plates in contact with each other) conditions. The short circuit measured the residual impedance in the test leads, and the open circuit measured the combined effect of the stray admittance and the residual impedance (see Figs. 2*b* and 2*c*). Impedance measurements of highly conductive specimens may be significantly affected by cable inductance, $Z_L = L_{cable}\omega$ (often at frequencies greater than 100 kHz). Inductance may also cause resonance in the MHz frequency range.

Data Reduction (Standard Procedure)

Impedance data were interpreted based on a parallel-plate capacitor model. The relationship between the capacitance, C^*, of a lossy capacitor and the complex permittivity, κ^*, of a material is:

$$C^* = \kappa^* C_o = \kappa^* \frac{\epsilon_o A}{L} \tag{9}$$

where A is the cross-sectional area of the plate, L is the distance between the plates, C_o is the capacitance of the same capacitor in vacuum, κ^* is the relative complex permittivity of the medium, and $\kappa^* = \epsilon^*/\epsilon_o = \kappa'\text{-}j(\kappa'' + \sigma/\omega\epsilon_o)$. Polarization losses are represented by κ'' and conduction losses are represented by the term $\sigma/\omega\epsilon_o$.

A lossy capacitor is represented by a capacitor in parallel with a resistor. The admittance, $Y = 1/Z$, of a lossy capacitor is:

$$Y_c^* = j\omega C^* = j\omega\kappa^* C_o \tag{10}$$

Then:

$$Y_c^* = j\omega\frac{A\epsilon_o}{L}\left[\kappa' - j\left(\kappa'' + \frac{\sigma}{\omega\epsilon_o}\right)\right] = \left(\kappa'' + \frac{\sigma}{\omega\epsilon_o} + j\kappa'\right)\omega\frac{A\epsilon_o}{L} \tag{11}$$

Finally, the expressions for the real and the imaginary permittivity are:

$$\kappa' = \frac{\mathrm{Im}(Y_c^*)L}{\omega\epsilon_o A} \tag{12}$$

$$\kappa'' + \frac{\sigma}{\omega\epsilon_o} = \frac{\mathrm{Re}(Y_c^*)L}{\omega\epsilon_o A} \tag{13}$$

It is assumed that Y_c^* has been corrected for stray and residual impedances, but not for the series interfacial impedance at the electrode.

Limiting Frequency

The minimum frequency at which electrode polarization does not significantly affect real permittivity measurements is herein called the "limiting frequency." This frequency can be determined by modeling the electrode-material system as a pure capacitor (simplest model of a blocking electrode) in series with a lossy capacitor that represents the material, as shown in Fig. 3 (Klein and Santamarina 1996). The complex admittance of this circuit is:

$$Y^*_{\mathrm{circuit}} = \frac{1}{\left(\frac{A\sigma_s}{L_s} + j\omega\frac{A\kappa_s'\epsilon_o}{L_s}\right)^{-1} - j\frac{L_e}{\omega A\epsilon_o}} \tag{14}$$

where σ_s is specimen conductivity, κ_s' is specimen real permittivity, L_s is specimen length, L_e is the equivalent thickness of the capacitor formed by the accumulation of ions at the electrode, and A is the cross-sectional area of the specimen. The "computed permittivity" is obtained by equating the admittance of a lossy capacitor (Eq 11) with the circuit admittance (Eq 14). Assuming $L_s >> L_e$:

$$\kappa' = \frac{\mathrm{Im}(Y^*_{\mathrm{circuit}})\cdot L_s}{\omega\epsilon_o A} = \frac{\left(\frac{\sigma_s}{\epsilon_o\omega}\right)^2\frac{L_e}{L_s} + \kappa_s'}{1 + \left(\frac{L_e}{L_s}\right)^2\left(\frac{\sigma_s}{\epsilon_o\omega}\right)^2} \tag{15}$$

The limiting frequency can be determined from Eq 15 by defining a level of acceptable error in the real permittivity measurement, $e_\kappa = (\kappa' - \kappa_s')/\kappa_s'$:

$$\omega_{\mathrm{limit}} = \frac{\sigma_s}{\epsilon_o}\sqrt{\frac{L_e}{L_s}\cdot\frac{1}{\kappa_s'\cdot e_\kappa}} \tag{16}$$

where κ' is the measured real permittivity and κ_s' is the true material permittivity. The limiting frequency ω_{limit} is proportional to the conductivity of the material; therefore, highly conductive specimens will be affected by electrode polarization to higher frequencies than low-conductivity materials.

In order to verify the adequacy of the model, Eq 16 was used to calculate the limiting frequencies for impedance measurements of three aqueous electrolytes of different conductivities. The computed limiting frequencies closely fit the measured data (Klein and Santamarina 1996).

The simplicity of the proposed electrode model enables the closed-form derivation of the equation for the limiting frequency (Eq 16). A more complex model, which includes specimen-electrode interactions (e.g., redox reactions and ionic diffusion), will be discussed later in the paper.

Four-Terminal Electrode Systems (Hz-MHz)

Four-terminal electrode systems use separate current injection and potential monitoring electrodes to avoid the effects of electrode polarization (Fig. 4). There are two underlying concepts in this method: first, current is the same everywhere in the system due to continuity, and second, the potential is measured within the specimen, away from the charge transfer process occurring at the current injection electrodes. The electrochemical charge transfer process occurring at the potential electrodes is minimized through the use of high-input impedance amplifiers, which reduce the current through these electrodes to a level below the required

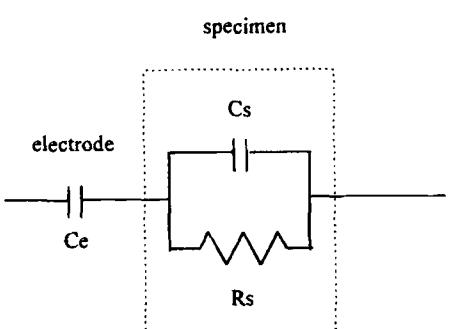

FIG. 3—*Simple circuit to model electrode polarization effects: a lossy capacitor in series with a capacitor.*

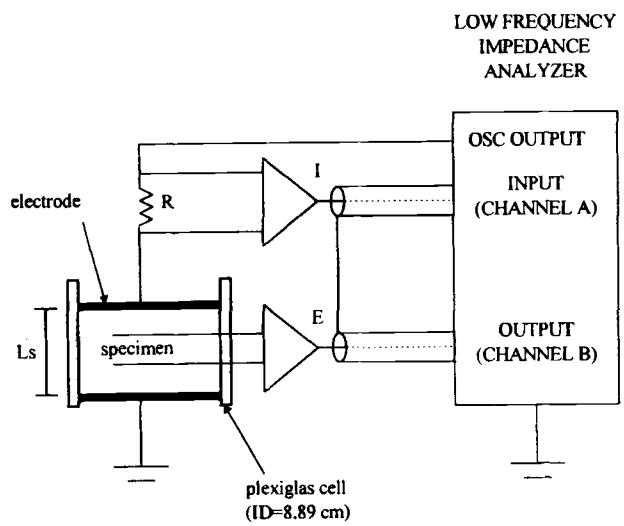

FIG. 4—*Four-electrode system:* I *is the measured current and* E *is the measured potential drop.*

threshold to initiate faradaic charge transfer processes (Olhoeft 1981).

Four-terminal measurements are typically conducted in frequency sweep mode. Nakamura et al. (1981) performed time domain spectrometry using a Fourier-synthesized pseudo-random noise excitation. In this case, measurements are acquired simultaneously for all frequencies, thereby avoiding biases due to thermal drift.

Experimental Setup

The four-terminal system used in this study was based on the same specimen holder used in the two-terminal system. The additional potential electrodes consisted to two wires placed at one third and two thirds of the specimen height. The circular end electrodes (current electrodes; diameter = 8.89 cm) applied a signal to the specimen, while the intermediate wire electrodes (potential electrodes) measured the voltage drop.

The same HP-4192A low-frequency impedance analyzer was used to obtain amplitude/phase data at frequencies between 5 Hz and 13 MHz (Fig. 4). The oscillator of the HP-4192A was utilized as a high-current input terminal. The HP-4192A was connected to the specimen holder through two differential amplifiers (input impedance $> 10^9$ ohms). One differential amplifier was connected to Channel B of the HP-4192A to measure the voltage drop between the potential electrodes. The other amplifier was connected to Channel A of the HP-4192A to measure the voltage drop across a resistor of known magnitude, $R = 1$ kΩ, from which the current I was calculated. The HP-4192A compared the two signals to obtain relative amplitude and phase data.

Calibration

The transfer function of the amplification-measurement system (i.e., frequency-dependent gain and phase shift) was determined and removed from the measurements. The amplifiers were designed to have a gain of four and zero phase shift for frequencies less than 10^6 Hz. The actual transfer function, T, of the amplification-measurement system was determined as the ratio of measured impedance, Z_m, to the true impedance, Z, of calibration circuits connected to the amplifiers simulating the specimen (Fig. 5*a*):

$$T = \frac{Z_m}{Z} = \frac{R_m + jX_m}{R + jX} \tag{17}$$

where R_m and X_m are the measured resistance and reactance, and R and X are the actual resistance and reactance of the circuits used for calibration. Seven circuits of known impedances were used for calibration over the frequency range of 5 Hz to 13 MHz. Typical calibration data are presented in Fig. 5*b*.

Data Reduction

The specimen impedance was determined from the amplitude/phase measurements. The measured gain/loss between Channels A and B in dB, $(B - A)_m$, is:

$$(B - A)_m = 20 \log \frac{|V_B|}{|V_A|} \tag{18}$$

where the subscript "m" denotes a measured value. The voltage drop across the known resistor ($R = 1$ kΩ) is $|V_A| = V_A = R \cdot I$, where I is the current flowing across the resistor and the specimen. The measured amplitude of the impedance of the system is $|Z^*_m| = |V_B|/I$:

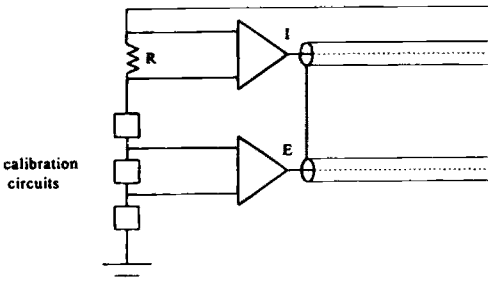

(a)

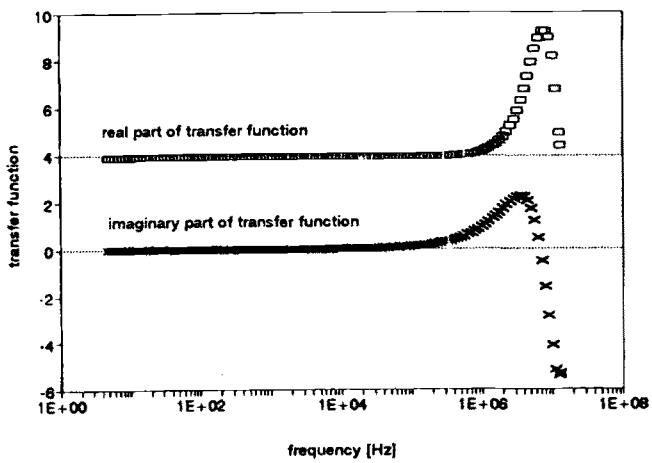

(b)

FIG. 5—(a) *Calibration of the four-terminal device with "calibration circuits";* (b) *transfer function determined with three 10-kΩ resistors in series.*

$$(B - A)_m = 20 \log \frac{|V_B|}{R \cdot I} = 20 \log \frac{|Z^*_m|}{R} \tag{19}$$

Rearranging Eq 19 and solving for the measured impedance:

$$|Z^*_m| = R \cdot 10^{(B-A)_m/20} \tag{20}$$

The complex impedance of the material is computed with the measured phase angle:

$$Z^*_m = |Z^*_m| \cdot (\cos \theta_m + j \sin \theta_m) \tag{21}$$

The actual impedance of the specimen is the measured impedance Z^*_m divided by the transfer function of the amplifiers T,$Z^* = Z^*_m/T$. After the impedance of the specimen is determined, permittivity values are calculated using the relationship between total current density through the specimen J_{tot}, conduction current density J_c, and displacement current density J_d:

$$J_{tot} = J_c + J_d \tag{22}$$

The current densities are functions of material conductivity σ, permittivity ϵ^*, the electric field E, and the angular frequency ω:

$$J_c = \sigma E \tag{23}$$

$$J_d = j\omega\epsilon_o\kappa^*E = j\omega\epsilon_o(\kappa' - j\kappa'')E \quad (24)$$

Substituting Eqs 23 and 24 into Eq 22:

$$J_{tot} = \sigma E + j\omega\epsilon_o(\kappa' - j\kappa'')E = \omega\epsilon_o E\left[\left(\frac{\sigma}{\omega\epsilon_o} + \kappa''\right) + j\kappa'\right] \quad (25)$$

Taking into consideration the cross-sectional area of the specimen A and the distance between potential electrodes L, $I_{tot} = J_{tot}/A$ and $E = \Delta V/L$:

$$\omega\epsilon_o\left[\left(\kappa'' + \frac{\sigma}{\omega\epsilon_o}\right) + j\kappa'\right] = \frac{I_{tot}}{\Delta V}\cdot\frac{L}{A} \quad (26)$$

Substituting $Z^* = \Delta V/I_{tot}$ into Eq 26:

$$\omega\epsilon_o\left[\left(\kappa'' + \frac{\sigma}{\omega\epsilon_o}\right) + j\kappa'\right] = \frac{1}{Z^*}\cdot\frac{L}{A} = \frac{L}{A} \cdot \frac{T}{R\cdot 10^{(B-A)_m/20}(\cos\theta_m + j\sin\theta_m)} \quad (27)$$

Equating real and imaginary parts:

$$\kappa' = \frac{L}{\omega\epsilon_o A}\left(\frac{-T\sin\theta_m}{R\cdot 10^{(B-A)_m/20}}\right) \quad (28)$$

$$\kappa'' + \frac{\sigma}{\omega\epsilon_o} = \frac{L}{\omega\epsilon_o A}\left(\frac{T\cos\theta_m}{R\cdot 10^{(B-A)_m/20}}\right) \quad (29)$$

Limiting Frequency

Assuming that electrode polarization does not occur, the ability of the four-terminal system to accurately measure the real permittivity of a material is restricted by the adequacy of the measurement device (the HP-4192A in this study) to resolve small-phase angles θ at low frequencies. The loss tangent of the material, $\tan\delta = (\kappa'' + \sigma/\omega\epsilon_o)/\kappa'$, is directly related to the phase angle (from Eqs 28 and 29):

$$\tan\delta = \frac{\kappa'' + \sigma/\omega\epsilon_o}{\kappa'} = -\frac{1}{\tan\theta} \quad (30)$$

The limiting frequency ω_{limit} at which the phase angle can be measured accurately is found by assuming $\kappa'' << \sigma/\omega\epsilon_o$ at low frequencies and solving Eq 30 for ω:

$$\omega_{limit} = \frac{\sigma\cdot|\tan\theta_{min}|}{\epsilon_o\cdot\kappa'} \quad (31)$$

where σ is specimen conductivity, κ' is specimen permittivity, and θ_{min} is the smallest phase angle that can be measured accurately with a specific device (Klein 1995).

Comparing Two-Terminal and Four-Terminal Systems

The relationship between the two-terminal and the four-terminal limiting frequencies is (Eqs 16 and 31):

$$\frac{\omega_{2T}}{\omega_{4T}} = \frac{\sqrt{\frac{L_e}{L_s}\cdot\frac{1}{e_\kappa}}\cdot\sqrt{\kappa'_s}}{|\tan\theta_{min}|} \quad (32)$$

Considering parameters relevant to this study ($\theta_{min} = 5\cdot 10^{-3}$ rad, $L_e/L_s = 10^{-7}$, and $e_\kappa = 10\%$), Eq 32 becomes:

$$\frac{\omega_{2T}}{\omega_{4T}} = \frac{\sqrt{\kappa'_s}}{5} \quad (33)$$

Therefore, the limiting frequency for the two-terminal method is higher than the limiting frequency for the four-terminal method by a factor of $\sqrt{\kappa'_s}/5$. Note that θ_{min} for the HP-4192A is a function of frequency and the input level of each channel.

Coaxial Systems (MHz-GHz)

A coaxial termination probe can be used to determine the complex reflection coefficient from the surface of the specimen. The complex permittivity of the medium is computed from the measured reflection coefficient. Waveguides and coaxial transmission lines with two ports have been used to determine the complex transmission coefficient (Chew et al. 1991). If transmission and reflection coefficients are determined, both the permittivity and the permeability of the material can be computed.

Experimental Setup

An HP-8752A network analyzer was used in conjunction with an HP-85070A dielectric coaxial termination probe to measure the complex permittivity of the specimens in the frequency range between 20 MHz to 1.3 GHz (Fig. 6). Computer software was used with the probe to control the network analyzer, measure the complex reflection coefficient of the probe in contact with the specimen, and calculate the complex dielectric permittivity. This software can display the results in a variety of graphical and tabular formats (Hewlett-Packard 1991). Good contact between the specimen and probe is very important as air gaps or fluid segregation will cause erroneous measurements.

Calibration

This high-frequency system is calibrated by measuring open circuit (air), short circuit (metallic shorting block), and deionized water.

Measurements of Soil-Water Mixtures

Broad-band complex permittivity data of soil-water mixtures were obtained using the low-frequency two-terminal and four-

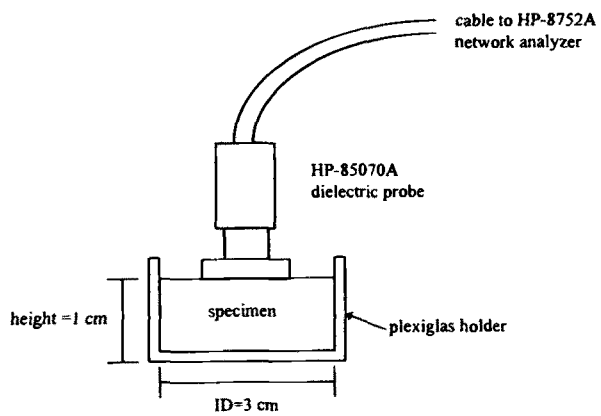

FIG. 6—*Coaxial termination system.*

terminal systems described previously (5 Hz to 13 MHz) and the high-frequency coaxial termination system (20 MHz to 1.3 GHz).

Materials—Specimen Preparation

Measurements were performed on quartz sand, kaolinite clay, and bentonite clay at three different moisture contents (for clarity of plots, data are presented for two selected moisture contents). These soils were chosen to provide a wide range of material parameters, e.g., relevance of double layer phenomena. Table 1 summarizes the relevant characteristics of these three soils; the significant differences in specific surface should be noted. The characteristics of the six specimens are presented in Table 2.

TABLE 1a—*Characteristics of tested sand.*

	Ottawa 20–30
Predominant material	Quartz
Grain shape angularity	Bulky
Specific gravity	2.65
D_{10}, mm	0.60
D_{50}, mm	0.72
D_{60} mm	0.75
D_{90} mm	0.83
$Cu = D_{60}/D_{10}$	1.25
e_{max}	0.738
e_{min}	0.501
$e_{max} - e_{min}$	0.237
Estimated specific surface, m^2/g	$3.14 \cdot 10^{-3}$

TABLE 1b—*Characteristics of tested clays.*

	Kaolinite	Bentonite
Source	Vanderbilt Co., Los Angeles,	Saskatchewan, Canada
Trade name	Peerless clay	Avonseal/Geoseal
Color	light cream	light tan
Specific gravity	2.6	2.55
Specific surface, m^2/g	10	400
Liquid Limit[a], %	50	250
Plastic Limit[a], %	35	50
Main cation[b]	sodium	sodium
CEC, meq/100 g	20–30	80–85
pH value[c]	4.8 (10% solids)	9.0 (5% solids)
Conductivity[c], S/m	0.004 (10% solids)	0.112 (5% solids)

[a]University of Waterloo—standard ASTM procedure.
[b]University of Waterloo—ion chromatography on extracted fluid (bentonite: centrifuge; kaolinite: filtration).
[c]University of Waterloo—solids in suspension.

The quartz sand was washed with deionized water to remove fines and excess salts. The three soils were mixed with deionized water to obtain specimens of various moisture contents. The prepared moist soils were placed in the test cells by scooping and lightly tamping. The moisture content of each specimen was determined immediately after electromagnetic measurements were completed.

Results—General Trends

Figures 7 to 9 present two-terminal, four-terminal, and coaxial probe data for the various specimens. Data are presented using log-log graphs to the same scale. This format facilitates comparison of different materials while permitting the visualization of measurement errors at low frequencies. Computed limiting frequencies for the two-terminal and four-terminal real permittivity measurements are also shown (see Table 2).

General trends in real permittivity, losses ($\kappa'' + \sigma/\omega\epsilon_0$), and "effective conductivity" ($\kappa''\omega\epsilon_0 + \sigma$) data are evident for all soil-water mixtures:

- Electrode polarization is shown in two-terminal measurements as increasing κ' with decreasing frequency below the limiting frequency. Four-terminal measurements also show increasing κ' with decreasing frequency at low frequencies ($\theta_{measured}$ remains at θ_{min} until it begins alternating randomly between $-\theta_{min}$ and $+\theta_{min}$).
- Free water polarization is evident in the saturated sand and kaolinite specimens as an increase in $\kappa'' + \sigma/\omega\epsilon_0$ at $f >\approx 3 \cdot 10^8$ Hz. A corresponding decrease in κ' is present, yet it is not obvious due to the scale of the κ' plot. Free water polarization is not noticeable at high frequencies in bentonite specimens because the trend is overwhelmed by the tail end of polarizations that occur at lower frequencies (e.g., double layer and Maxwell-Wagner polarizations).
- The losses ($\kappa'' + \sigma/\omega\epsilon_0$) are fairly constant at low frequencies, but clearly increase at high frequencies due to free water polarization losses.
- Both the "effective conductivity" and the real permittivity of the soil-water mixtures increase as the water content increases towards saturation.

Electrode Polarization (Two-Terminal and Four-Terminal)

The impact of electrode polarization on two-terminal measurements was determined by inverting for the equivalent thickness

TABLE 2—*Specimen characteristics.*

Soil	*wc*, %	Wet Unit Weight, kN/m^3	2T L_m,[a] cm	σ_{dc}, S/m	κ' $f = 10^7$ Hz	κ' $f = 10^4$ Hz	2T L_e,[b] m	2T f_{limit},[c] Hz $e = 1\%$	4T f_{limit},[d] Hz $\theta = 5$ mrad
Quartz sand	2.4	N/A	0.8	$1.7 \cdot 10^{-4}$	2	20	$10^{-8.5}$	$4.3 \cdot 10^3$	917
	15.7	N/A	1.3	$3.5 \cdot 10^{-3}$	30	60	$10^{-9.4}$	$1.4 \cdot 10^4$	$5.2 \cdot 10^3$
Kaolinite	0.8	5.5	3.50	10^{-8}	3	3	$10^{-3.1}$	156	0.3
	54.0	15.3	3.70	$4.7 \cdot 10^{-3}$	40	10^3	$10^{-9.3}$	$1.6 \cdot 10^4$	$1.1 \cdot 10^4$
Bentonite	9.5	10.0	3.60	10^{-4}	4	400	10^{-7}	$1.5 \cdot 10^4$	$2.2 \cdot 10^3$
	180.5	15.6	4.00	0.065 (2T) 0.74 (4T)	50	N/A	$10^{-9.6}$	$1.5 \cdot 10^6$	$1.3 \cdot 10^6$

NOTE: N/A = information not available.
[a]Two-terminal sample thickness.
[b]Two-terminal equivalent capacitor thickness (see text for details).
[c]Computed with Eq 16.
[d]Computed with Eq 31.

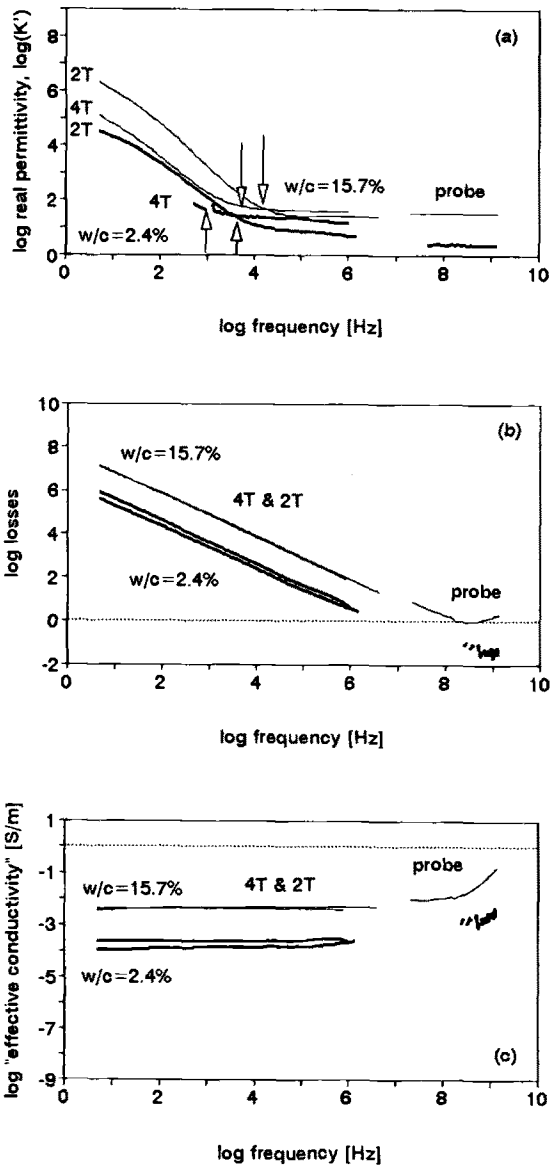

FIG. 7—*Sand (water content = 2.4 and 15.7%): two-terminal 2T, four-terminal 4T, and coaxial probe data:* (a) *real relative permittivity;* (b) *losses* ($\kappa'' + \sigma/\omega\epsilon_0$); *and* (c) *"effective conductivity"* ($\kappa''\omega\epsilon_0 + \sigma$). *Arrows indicate limiting frequency for each measurement. Note the poor performance of the four-terminal system for specimens with low moisture content.*

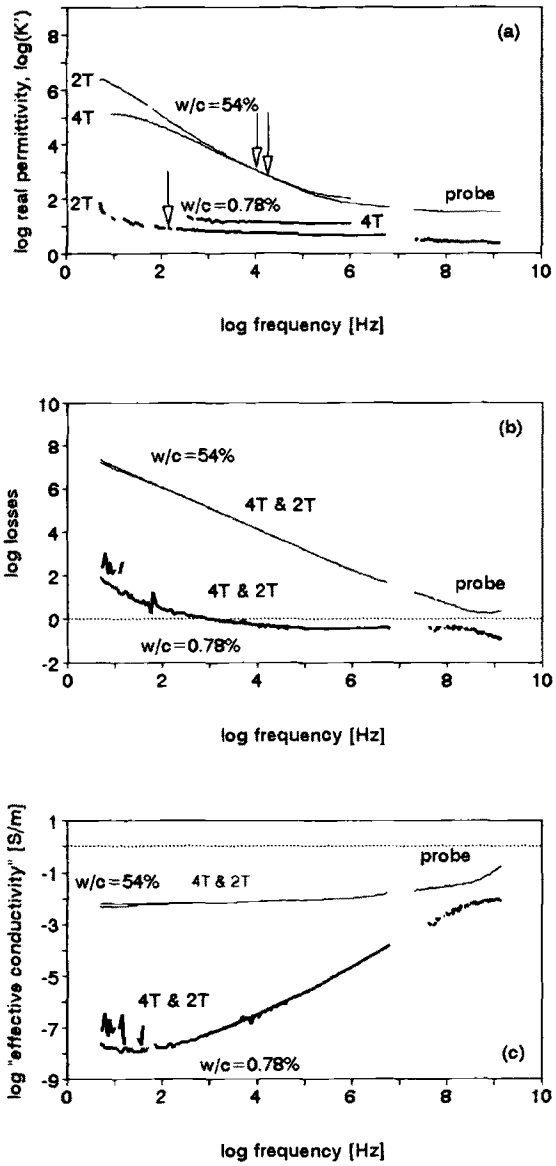

FIG. 8—*Kaolinite (water content = 0.78 and 54%): two-terminal 2T, four-terminal 4T, and coaxial probe data:* (a) *real relative permittivity;* (b) *losses* ($\kappa'' + \sigma/\omega\epsilon_0$); *and* (c) *"effective conductivity"* ($\kappa''\omega\epsilon_0 + \sigma$). *Arrows indicate limiting frequency for each measurement. Note the poor performance of the four-terminal system for specimens with low moisture content.*

of the capacitor formed by the accumulation of ions at the electrode L_e (see Table 2). The thickness was obtained by fitting Eq 15 to the measured spectral response. Computed L_e values decreased significantly when water was added to the specimens, which implies that this thickness L_e also represents air gaps at the electrode-specimen interface. Furthermore, L_e values varied for specimens of different particle size, length, degree of saturation, and conductivity. It is probable that L_e also varies with the amount of applied pressure. Because the thickness of the ion layer depends on specimen length, the suggested method of measuring the impedance of two specimens of different lengths to cancel the electrode polarization impedance will not produce accurate results (see, for example, Schwan et al. 1962; Hill et al. 1969).

It is possible that some electrode polarization may take place at the potential electrodes in the four-terminal system (Nakamura et al. 1981).

Phase Angle Resolution (Four-Terminal)

The increase in four-terminal κ' values at low frequencies occurred due to inaccuracies in phase measurements with the HP-4192A (Figs. 7*a* and 8*a*; sand *wc* = 15.7% and kaolinite *wc* = 54%). Manufacturer's specifications show that accuracy in θ depends on frequency and input level of each channel. The magnitude of the measured phase angles decreases with decreasing frequency due to Ohmic losses. As θ approaches zero, measured phase angles fluctuated between the positive and the negative value of phase resolution.

Specimen Conductivity

The conductivity of the specimen plays a crucial role in defining the frequency range of a measurement system (i.e., ω_{limit} in the

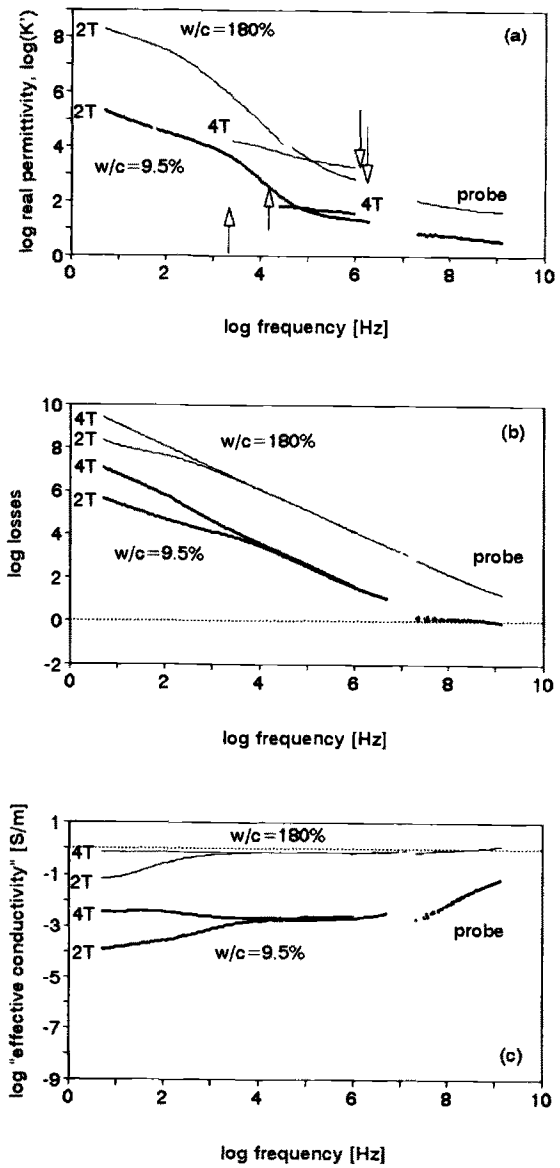

FIG. 9—*Bentonite (water content = 9.5 and 180%): Two-terminal, four-terminal 4T, and coaxial probe data:* (a) *real relative permittivity;* (b) *losses* ($\kappa'' + \sigma/\omega\epsilon_o$)*; and* (c) *"effective conductivity"* ($\kappa''\omega\epsilon_o + \sigma$)*. Arrows indicate limiting frequency for each measurement.*

two-terminal and four-terminal systems). Conductivity also controls other phenomena that occur during testing such as fringe/edge effects and surface conduction. Fringe/edge effects are minimized in highly conductive, small-thickness specimens. Surface conduction errors are magnified in specimens with high material conductivity and slender geometry.

Small-thickness and large-diameter specimens can be tested readily in two-terminal parallel electrode systems. However, specimens with a slender geometry must be used for four-terminal measurements to permit the installation of potential electrodes.

Inductance

Two-terminal measurements are affected at MHz frequencies by inductance in the peripherals. Figure 7*a* shows lower κ' values for the two-terminal measurements of sand (wc = 15.7%) than for the four-terminal and coaxial probe data at frequencies greater than approximately 10^4 Hz. The frequency at which inductance begins to affect the measurements decreases as the conductivity of the specimen increases (i.e., the material is "shorted-out" of the circuit). In this case, calibration in short becomes crucial yet not always completely efficient. One method of correcting the two-terminal data for inductance is to model the measured values as a lossy capacitor in series with an inductor and match the high-frequency ($f >\approx 10^5$) κ' values of the two-terminal data to the coaxial probe data.

Other Measurement Problems

Moisture migration and fluid "bleeding" in wet sands affect the three measurement procedures. There are also restrictions on the maximum diameter of particles relative to the size of the fixture, e.g., diameter of waveguide in the coaxial probe.

More Complex Electrode Model

Copper electrodes were used in this study, allowing redox reactions to take place. Furthermore, ionic diffusion occurred at the electrode-specimen diffuse layer. The simple electrode model (a single capacitor) used to derive Eq 16 may be improved to better describe the measurements. Two circuit elements were added to the electrode capacitance C_e: a resistance R_e to represent redox reactions and a constant phase element Q to represent ionic diffusion (Fig. 10). The admittance of the constant phase element Y_Q^* is:

$$Y_Q^* = M\omega^\beta + jN\omega^\beta \qquad (34)$$

where M, N, and β are fitting parameters (Raistrick et al. 1976). The M parameter significantly affects the shape of the imaginary permittivity curve, and the N parameter controls the shape of the real permittivity curve. Infinite electrode resistance, $R_e \rightarrow \infty$, means that redox reactions are not occurring at the electrode-material interface.

The resolvability of the model parameters is shown in Fig. 11: two-terminal (5 Hz to 13 MHz) and coaxial probe (20 MHz to 1.3 GHz) measurements of a 1.8 mmol/L NaCl solution. These plots show the change in the average error between measured κ'_{meas} and modeled κ'_{model} values of real permittivity as each parameter is varied, holding the other parameters constant at their optimum values. The average error for n measurements is expressed as:

$$\text{percent error } \kappa' = \frac{1}{n}\left(\sum \frac{|\kappa'_{meas} - \kappa'_{model}|}{\kappa'_{meas}}\right)100 \qquad (35)$$

The minimum average error is 1.6% at the optimum values of the

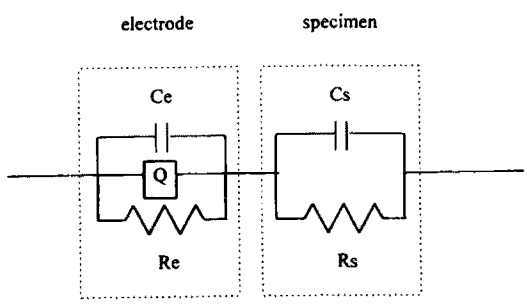

FIG. 10—*Enhanced circuit to model electrode polarization effects* (C_e, *oxidation-reduction reactions* R_e, *and ionic diffusion* Q)*. The lossy capacitor represents the material.*

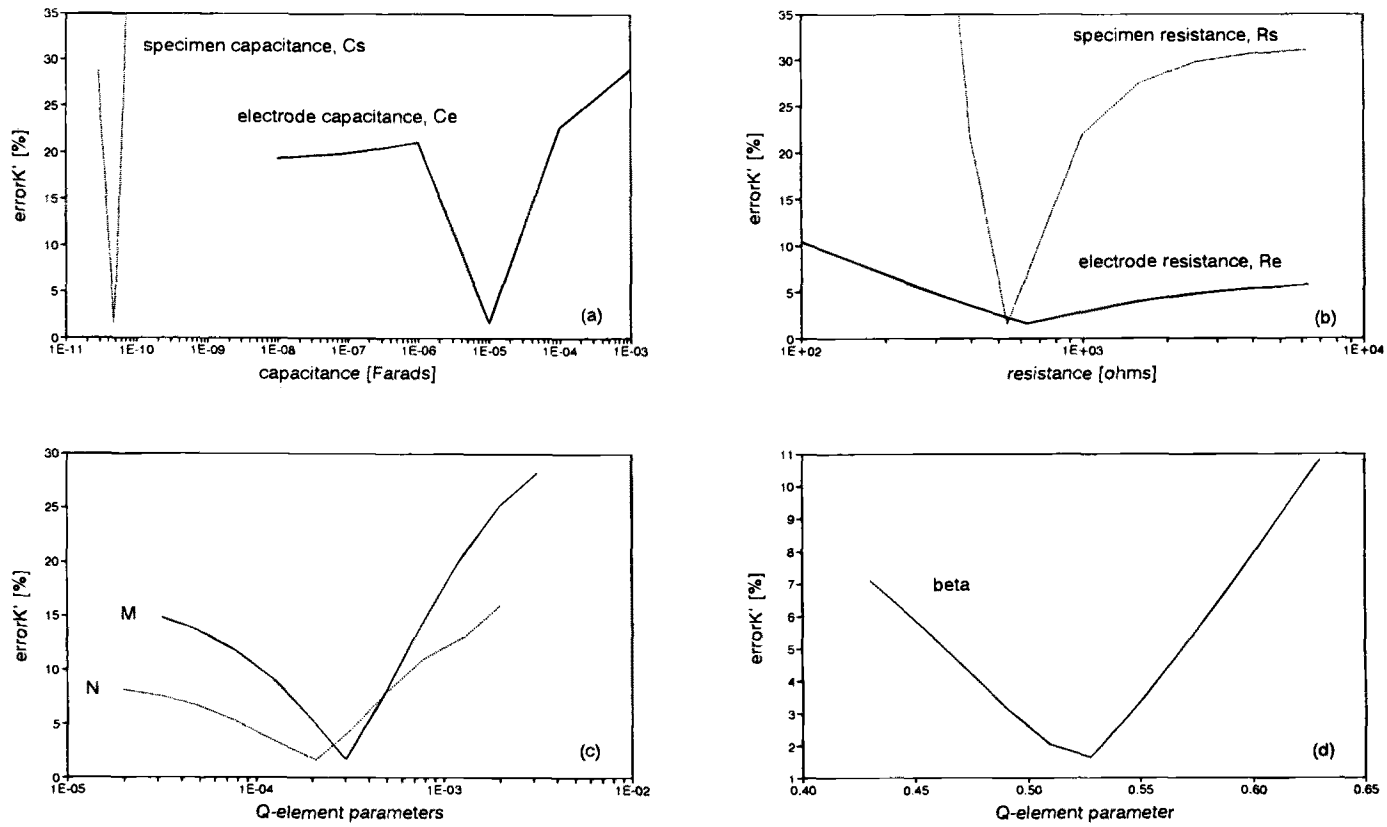

FIG. 11—*Resolvability of model parameters in Fig 10:* (a) C_e *and* C_s; (b) R_e *and* R_s; (c) M *and* N; (d) β.

parameters. The error increases significantly with variations in the parameters.

Electrode polarization affects not only real permittivity, but also the losses ($\kappa'' + \sigma/\omega\epsilon_0$) and the "effective conductivity" ($\kappa''\omega\epsilon_0 + \sigma$)for highly conductive specimens. While the four-terminal bentonite data show a constant variation of losses with frequency (on a log-log plot), the two-terminal data show a change of slope at low frequencies (Fig. 9). The circuit in Fig. 10 closely models this deviation from the hyperbolic σ/ω trend.

Conclusions

Different measurement techniques must be used to gather electromagnetic parameters over a wide frequency range. The high-frequency coaxial termination reflection procedure used in this study is easy to implement, produces reliable complex permittivity data, and can be used to characterize some properties of soil-water mixtures, e.g., moisture content. Low-frequency measurements can provide information about interactions between phases in multi-phase systems and double layer phenomena; however, low-frequency techniques are more cumbersome.

Electrode polarization affects two-terminal parallel plate measurements at low frequencies. Many techniques have been proposed to minimize or correct electrode polarization effects; the reliability of these methods is questionable. The minimum frequency (limiting frequency) at which electrode polarization does not significantly affect two-terminal measurements is a function of the conductivity, permittivity, and length of the specimen, as well as the thickness of the ion layer at the electrode-specimen interface. On the high-frequency end, two-terminal measurements are affected by the inductance of peripherals. The frequency at which inductance affects the measurements decreases as the conductivity of the specimen increases. Thus, accurate measurements of highly conductive specimens may not be possible with the two-terminal system. Two-terminal "effective conductivity" and losses were noticeably affected at the low-frequency end by electrode polarization for highly conductive specimens.

Four-terminal measurement systems minimize electrode polarization effects. Theoretically, four-terminal measurement systems can be used to obtain permittivity data at very low frequencies. However, the minimum frequency at which accurate measurements are obtained is a function of equipment accuracy for phase angle measurements relative to the loss tangent of the material.

The two-terminal limiting frequency is greater than the four-terminal limiting frequency by approximately $\sqrt{\kappa_s'}/5$.

Acknowledgments

This study is part of a research project on wave-geomedia interactions and applications that was initiated by the authors while they were at the University of Waterloo. Support from the Natural Science and Engineering Research Council of Canada and INCO is greatly appreciated. The authors are thankful to Victor Rinaldi and Moheb Fam for their valuable comments and suggestions.

References

ASTM Test Methods for A-C Loss Characteristics and Permittivity (Dielectric Constant) of Solid Electrical Insulating Materials (D 150-87), American Society for Testing and Materials, West Conshohocken, PA, 1987, pp. 24–34.

Chew, W. C., Olp, K. J., and Otto, G. P., "Design and Calibration of a Large Broadband Dielectric Measurement Cell," *IEEE Transactions on Geoscience and Remote Sensing*, Vol. 29, No. 1, 1991, pp. 42–47.

de Loor, G. P., "The Dielectric Properties of Heterogeneous Mixtures Containing Water," *IEEE Transactions on Geoscience and Remote Sensing*, Vol. GE-21, No. 3, 1983, pp. 364–369.

Fam, M. and Santamarina, J. C., "Study of Geoprocesses with Complementary Mechanical and Electromagnetic Wave Measurements in an Oedometer," *ASTM Geotechnical Testing Journal*, Vol. 18, No. 3, 1995, pp. 307–314.

Gross and McGehee, "The Layered-Capacitor Method for Bridge Measurements of Conductive Dielectrics," *IEEE Transactions on Electrical Insulation*, Vol. 23, No. 3, 1988, pp. 387–396.

Hewlett-Packard, *HP-85070A Dielectric Probe Kit*, Hewlett-Packard Company, CA, 1991.

Hill, N. E., Vaughan, W. E., Price, A. H., and Davies, M., *Dielectric Properties and Molecular Behaviour*, van Nostrand Reinhold Company Ltd., Toronto, 1969.

Klein, K., "Broad-Band Dielectric Permittivity Measurements," M.A.Sc. thesis, University of Waterloo, Waterloo, Ontario, 1995.

Klein, K. and Santamarina, J. C., "Polarization and Conduction of Clay-Water-Electrolyte Systems," discussion, *Journal of Geotechnical Engineering*, ASCE, Vol. 122, No. 11, November 1996, pp. 954–955.

Nakamura, H., Husimi, Y., and Wada, A., "Time Domain Measurement of Dielectric Spectra of Aqueous Polyelectrolyte Solutions at Low Frequencies," *Journal of Applied Physics*, Vol. 4, No. 4, 1981.

Olhoeft, G. R., "Chapter 9: Electrical Properties of Rocks," *Physical Properties of Rocks and Minerals*, McGraw Hill/CINDAS Data Series on Material Properties, McGraw-Hill Book Co., Toronto, 1981, pp. 257–329.

Parkhomenko, E. I., *Electrical Properties of Rocks*, Plenum Press, New York, 1967.

Raistrick, I. D., Ho, C., and Huggins, R. A., "Ionic Conductivity of Some Lithium Silicates and Aluminosilicates," *Journal of Electrochemical Society: Electrochemical Science and Technology*, Vol. 123, No. 10, 1976, pp. 1469–1476.

Santamarina, J. C. and Fam, M., 1997, "Dielectric Permittivity of Soils Mixed with Organic and Inorganic Fluids (0.02 GHz to 1.30 GHz)," *Journal of Environmental and Engineering Geophysics*, accepted for publication.

Schwan, Schwarz, Maczuk, and Pauly, "On the Low-Frequency Dielectric Dispersion of Colloidal Particles in Electrolyte Solution," *Journal of Physical Chemistry*, Vol. 66, 1962, p. 2626.

Scott, J. H., Carroll, R. D., and Cunningham, D. R., "Dielectric Constant and Electrical Conductivity Measurements of Moist Rock: A New Laboratory Method," *Journal of Geophysical Research*, Vol. 72, No. 20, 1967, pp. 5101–5115.

Sumner, J. S., *Principles of Induced Polarization for Geophysical Exploration*, Elsevier Scientific Publishing Company, New York, 1976.

von Hippel, A., *Dielectrics and Waves*, John Wiley & Sons, Inc., New York, 1954.

Ward, S. H., "Resistivity and Induced Polarization Methods," *Geotechnical and Environmental Geophysics—Investigations in Geophysics No. 5*, Society of Exploration Geophysicists, Tulsa, OK, 1992, pp. 147–189.